Supporting Information for

Ag-Doped Halide Perovskite Nanocrystals for Tunable Band Structure and Efficient Charge Transport

Shu Zhou[†], *Yaping Ma*[†], *Guodong Zhou*[‡], *Xin Xu*[‡], *Minchao Qin*[†], *Yuhao Li*[†], *Yao-Jane Hsu*[§], *Hanlin Hu*[I], *Gang Li*[I], *Ni Zhao*[‡], *Jianbin Xu*[‡], *and Xinhui Lu*[†,*]

[†] *Department of Physics, The Chinese University of Hong Kong, New Territories, Hong Kong*

[‡] *Department of Electronic Engineering, The Chinese University of Hong Kong, New Territories, Hong Kong*

[§] *National Synchrotron Radiation Research Center, Hsinchu, Taiwan*

[I] *Department of Electronic and Information Engineering, Hong Kong Polytechnic University, Hong Hum, Kowloon, Hong Kong*

E-mail: **xhlu@phy.cuhk.edu.hk*

Experimental Methods

Materials: All chemical reagents were employed directly as received: Lead (II) bromide ($PbBr_2$, Sigma-Aldrich, 99.999%, metals basis), cesium carbonate (Cs_2CO_3, Aladdin, 99.9%, metals basis), silver carbonate (Ag_2CO_3, Aladdin, 99.9%, metals basis), butylamine (BuAm, Aladdin, 99.5%), 2-propanol (IPrOH, Sigma-Aldrich, anhydrous, 99.5%), propionic acid (PrAc, Aladdin, 99.5%), hexane (HEX, Sigma-Aldrich, 95%), toluene (Sigma-Aldrich, anhydrous, 99.8%).

Preparing precursor solutions: $PbBr_2$ precursor solution was prepared by dissolving 184 mg (0.5 mmol) $PbBr_2$ in 1 ml 1:1:1 IPrOH:PrAc:BuAm, respectively. Cs-PrAc precursor solution was prepared by dissolving 163 mg Cs_2CO_3 (0.5 mmol) in 0.5 ml PrAc. For preparing Ag-PrAc precursor solution, 28 mg Ag_2CO_3 was firstly added into 2 ml PrAc. The mixture was stirred overnight, leading to the formation of a cloudy solution. The cloudy solution was then filtered through a PTFE filter (0.22 μm) and a clear Ag-PrAc solution (0.02 mmol) was obtained.

Synthesis of Ag^+-doped $CsPbBr_3$ NCs: The synthesis of undoped $CsPbBr_3$ NCs is adapted from that reported in previous literature.[34] Firstly, 20 μl Cs-PrAc was added into a mixed solution of hexane and 2-propanol (HEX:IPrOH = 2:1). The 100 μl $PbBr_2$ precursor was subsequently injected and the solution quickly turned green within a few seconds. The undoped $CsPbBr_3$ NCs were collected by centrifuging for 3 min at 2500 rpm and then re-dispersed in toluene. $CsPbBr_3$ NCs doped with Ag^+ were synthesized by adding different concentrations of Ag^+ precursor solution into the synthesis of undoped $CsPbBr_3$ NCs before

the NCs had formed. Firstly, 20 μl Cs-PrAc was added into a mixed solution of hexane and 2-propanol (HEX:IPrOH = 2:1). 20-80 μl Ag-PrAc precursor was then added into the mixed solution of hexane and 2-propanol that contains the Cs^+ precursor. Subsequently, the 100 μl $PbBr_2$ precursor was injected, leading to the formation of Ag^+-doped $CsPbBr_3$ NCs.

Characterizations: The Ag^+ concentration (molar ratio of Ag^+ to Pb^{2+}) of each doped $CsPbBr_3$ NCs was measured by using ICP-OES (Shimadzu ICPE-9820). TEM measurements were performed by FEI Tecnai Spirit microscope with an acceleration voltage of 200 kV. Samples for TEM measurements were prepared by drop-coating $CsPbBr_3$-NC-containing dispersion onto a carbon-coated copper grid. XPS and UPS measurements were performed at BL09A2 U5 beamline at the National Synchrotron Radiation Research Center, Taiwan. The excitation energy for XPS measurements was 750 eV. UPS measurements were carried out with a 21.2 eV He-Iα source and a −4 eV bias. Samples for XPS/UPS were prepared by dropcasting $CsPbBr_3$ NCs on a 8 mm × 8 mm FTO substrate. PL measurements were performed by using an integrating sphere in which a light-emitting diode excitation source was mounted. A UV-vis spectrometer (Hitachi U-3501) was used to measure the optical absorption of $CsPbBr_3$ NCs. Both PL and UV-vis measurements were carried out at a resolution of 1 nm. Time-resolved photoluminescence decay (TRPL) measurements were performed on $CsPbBr_3$ NCs that were dispersed in toluene by using an Edinburgh FLSP920 spectrophotometer equipped with an excitation source of 485 nm picosecond pulsed diode laser. GIWAXS measurements were carried out with a Xeuss 2.0 SAXS/WAXS laboratory beamline using a Cu X-ray source (8.05 keV, 1.54 Å) and a Pilatus3R 300K detector. The incidence angle is 0.2^o. STM measurements were performed at room temperature with an

Omicron scanning probe microscopy system. Samples for STM measurements were prepared by spin-coating a diluted $CsPbBr_3$-NC colloid onto a FTO substrate.

Fabrication of FETs: Heavily p-type Si substrates with thermally grown SiO_2 (300 nm) layer were cleaned by sonication in deionized water, isopropyl alcohol and acetone, followed by oxygen plasma treatment for 15 min. The Au interdigital electrodes were patterned by photolithography and a channel with a length (L) of 20 μm and width (W) of 15 mm was defined. A $CsPbBr_3$-NC film was then deposited by drop-casting the $CsPbBr_3$-NC colloid onto the Au electrodes pre-patterned on the Si/SiO_2 substrate. A small funnel was placed over the NC film to slow the evaporation.

Room temperature electrical measurements for the FETs were performed in a nitrogen-purged glove box under the dark condition by using a Keithley 2612 source meter. Low temperature electrical measurements were carried out in vacuum (10^{-3} pa) under the dark condition and a Scientific Instruments 9700 temperature Controller was employed. The cooling/heating rate was kept at about 1 K/min during the cooling/heating process. For the transfer/output measurements V_g/V_{ds} was applied in the pulse mode with period of 0.1 s and duty cycle of 0.5. When the continuous mode of operation was employed, the voltages were applied continuously during the scan.

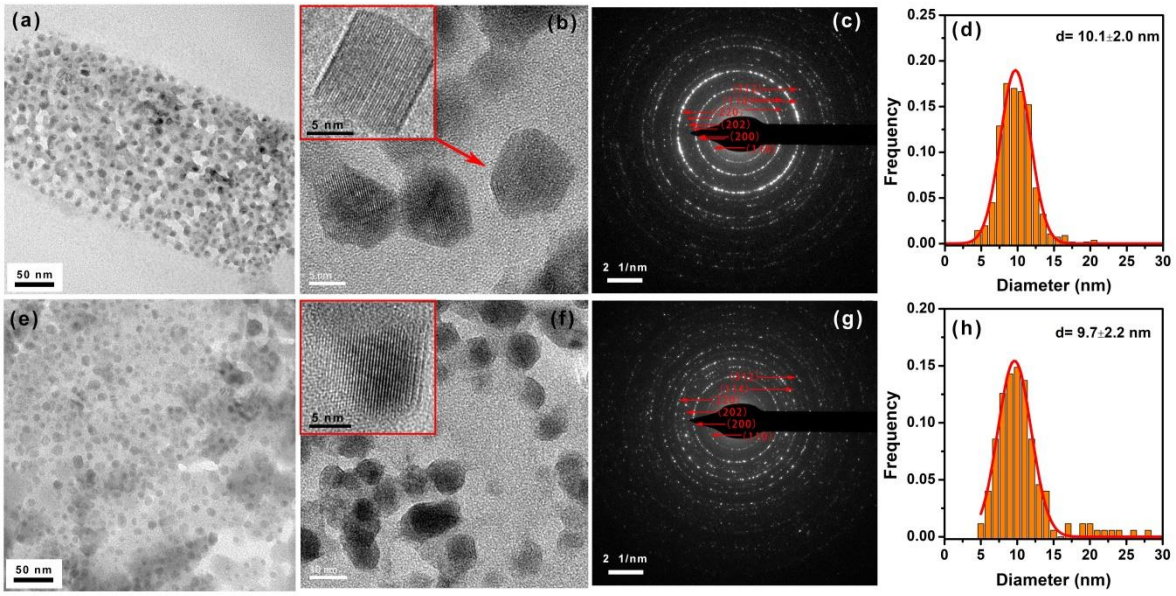

Figure S1. (a) TEM image, (b) HRTEM image, (c) associated selected area electron diffraction (SAED) image and (d) size distribution of undoped $CsPbBr_3$ NCs with a normal fit. The mean NC size is 10.1±2.0 nm. (e) TEM image, (f) HRTEM image, (g) associated selected area electron diffraction (SAED) image and (h) size distribution of Ag^+ doped $CsPbBr_3$ NCs with a normal fit. The mean NC size is 9.7±2.2 nm.

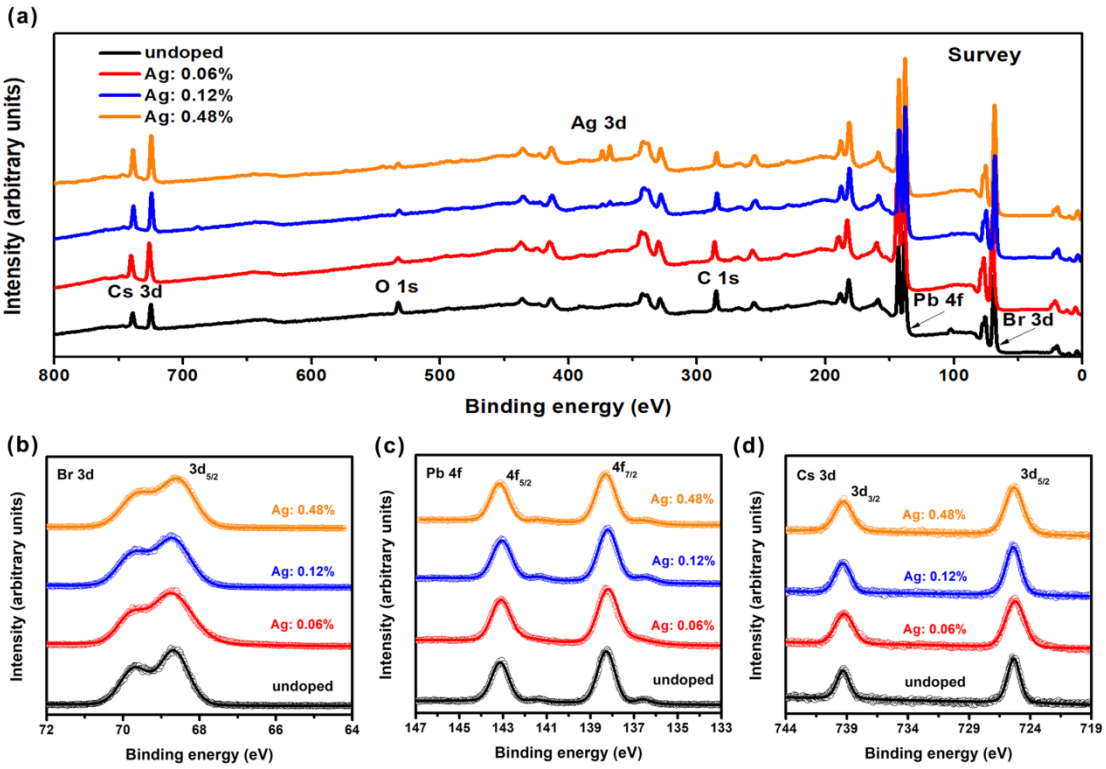

Figure S2. XPS results for undoped and Ag^{+}-doped $CsPbBr_3$ NCs. (a) Survey scan, (b) Br 3d, (c) Pb 4f, and (d) Cs 3d XPS spectra.

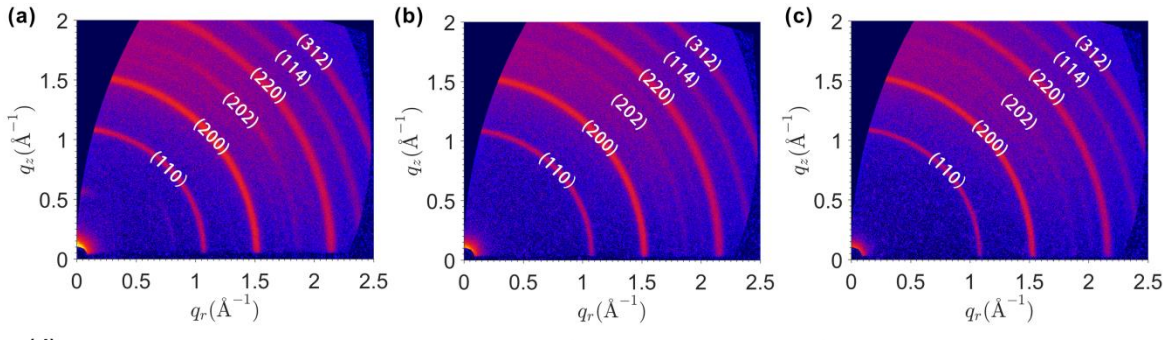

Figure S3. GIWAXS pattern of (a) undoped $CsPbBr_3$ NCs, (b) 0.23% Ag^+-doped $CsPbBr_3$ NCs and (c) 0.48% Ag^+-doped $CsPbBr_3$ NCs.

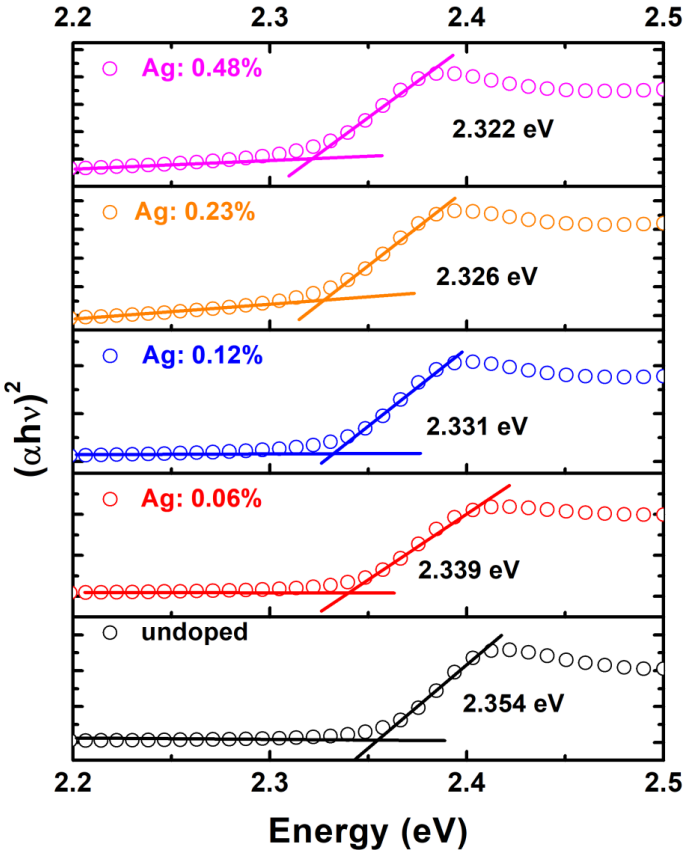

Figure S4. Tauc Plot of undoped $CsPbBr_3$ NCs and $CsPbBr_3$ NCs doped with different Ag^+ concentrations.

In line with previous reports[1,2], the $CsPbBr_3$ NCs is regarded as a direct-bandgap semiconductor when analyzing the optical absorption spectra.

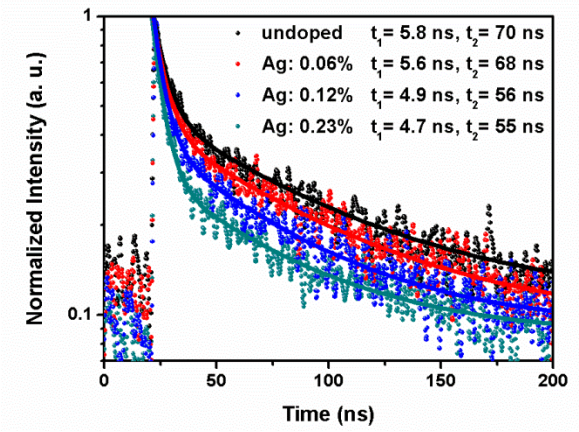

Figure S5. Time-resolved PL decay curves of undoped and Ag^+ doped $CsPbBr_3$ NCs for excitation at 485 nm. Both undoped and doped NCs exhibit biexponential decay with two lifetime components. The shorter lifetime (t_1) and longer lifetime (t_2) for each NC sample are indicated.

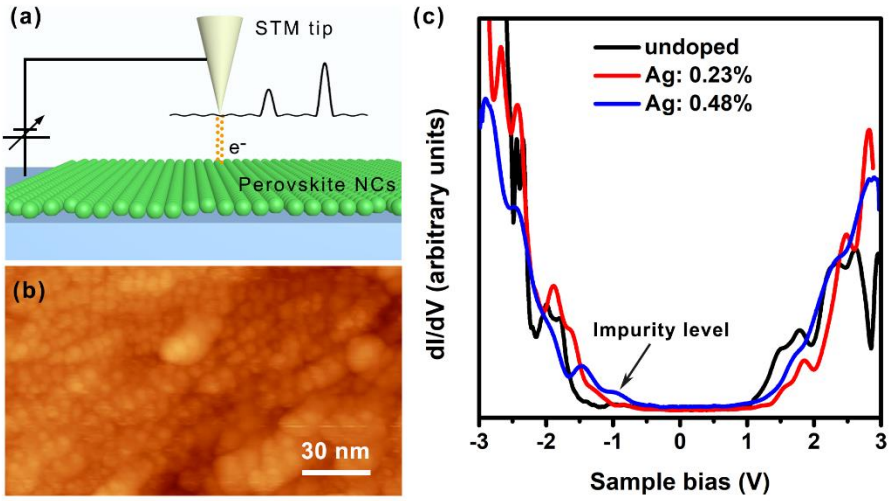

Figure S6. (a) Schematic of the STM setup for probing the electronic band structure of $CsPbBr_3$ NCs. (b) A representative STM image of a $CsPbBr_3$-NC film on which STS data were measured. (c) Tunneling spectra (dI/dV) for undoped and Ag^+-doped $CsPbBr_3$ NCs.

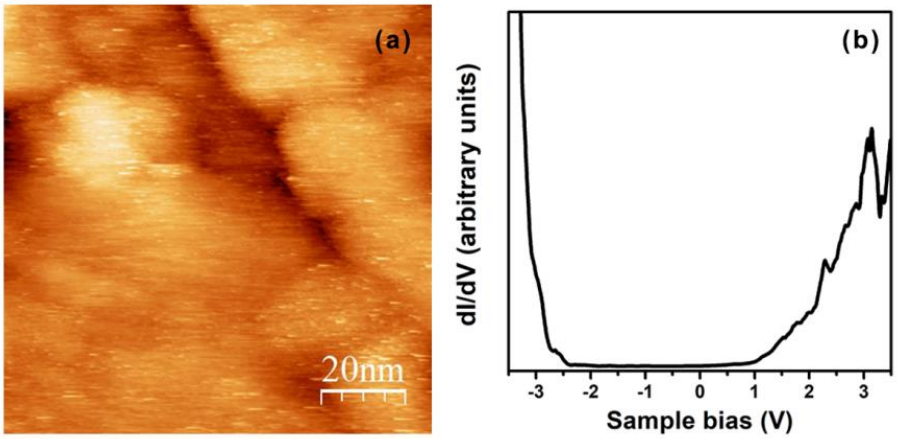

Figure S7. (a) STM image and (b) the associated STS spectrum for the FTO substrate.

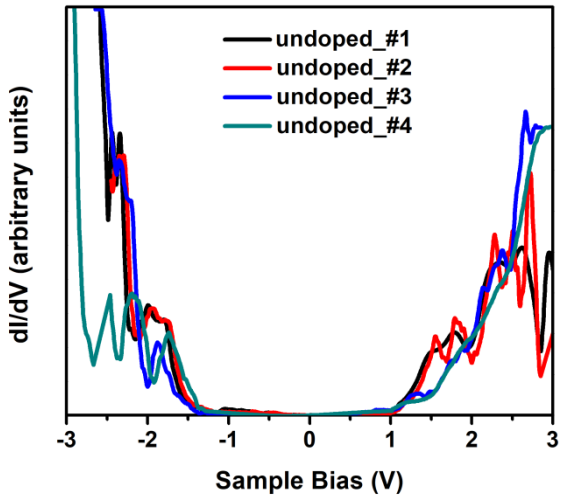

Figure S8. STS spectra collected from different $CsPbBr_3$ NCs for the undoped sample.

The impact of Ag^+ doping on the band structure of $CsPbBr_3$ NCs was also studied by Scanning Tunneling Spectroscopy (STS) measurements. As shown in Figure S6(a), the STM tip was placed above the $CsPbBr_3$ NCs on a fluorine-doped tin oxide (FTO) substrate to form a double-barrier tunnel junction.[3] Figure S6(b) presents a typical constant-current topographic STM image showing arrays of $CsPbBr_3$ NCs. The STM results for the pristine FTO substrate are shown in Figure S7. Figure S6(c) plots tunneling spectra (dI/dV) for undoped and Ag^+-doped $CsPbBr_3$ NCs, proportional to local density of states (DOS). Each spectrum is averaged over ~30 spectra of an individual NC to enhance the signal-to-noise ratio. A clear bandgap (zero-conductance) around the Fermi level (zero bias) can be identified for both undoped and Ag^+-doped $CsPbBr_3$ NCs. For undoped $CsPbBr_3$ NCs, doublet peaks were observed on both negative-bias and positive-bias sides of the spectrum, resulting from tunneling through $1S_{h/e}$ states in the valence band and the conduction band, respectively. For Ag^+-doped $CsPbBr_3$ NCs, these features were washed out, signifying the doping-induced perturbations to the pristine DOS. Remarkably, the valence band edge extends towards the Fermi Level with the increase of doping concentration, suggesting the presence of impurity levels. This is consistent with first-principle calculation results that the Ag-4d orbital

will hybridize with the Br-3p orbital, giving rise to a higher valence band edge.[4] It is noted that the presence of impurity levels leads to narrowing of the STS tunnelling gap are more serious than the red-shift of optical bandgap (E_{opt}) obtained from absorption. This can be due to the fact that the density of impurity states is much smaller than the original valence band states because the concentrations of Ag^{+} are not high (< 0.5%). The optical transition in doped $CsPbBr_3$ NCs largely originates from the original valence band states and the E_{opt} is not significantly reduced. However, these impurity states can be detected by STM/STS measurements despite the much lower density. This leads to the mismatch between the observed optical bandgaps and the STS tunneling gaps in doped $CsPbBr_3$ NCs. In addition, the STM measurements were performed on $CsPbBr_3$ NCs within the arrays, which may also make the STS bandgap smaller than the optical bandgap. Further explorations, such as with IR absorption measurements, might help understand the optical transitions in doped $CsPbBr_3$ NCs.[5]

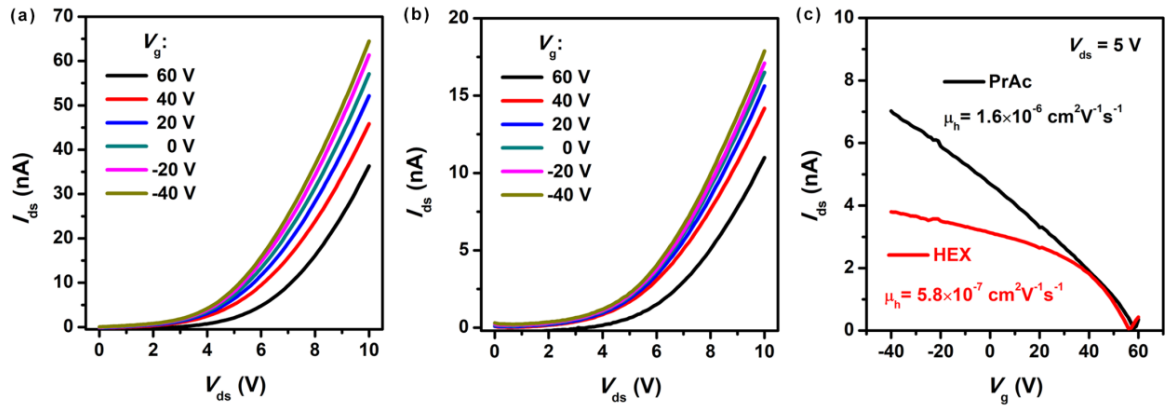

Figure S9. Output characteristics of FETs made with undoped $CsPbBr_3$ NCs treated by using (a) propionic acid (PrAc) and (b) hexane (HEX). (c) The associated transfer characteristics of the FET devices. It is found that surface treatments of $CsPbBr_3$ NCs does not contribute to the improvement of the charge transport properties. The hole mobilities are in the same order with the untreated undoped $CsPbBr_3$ NCs.

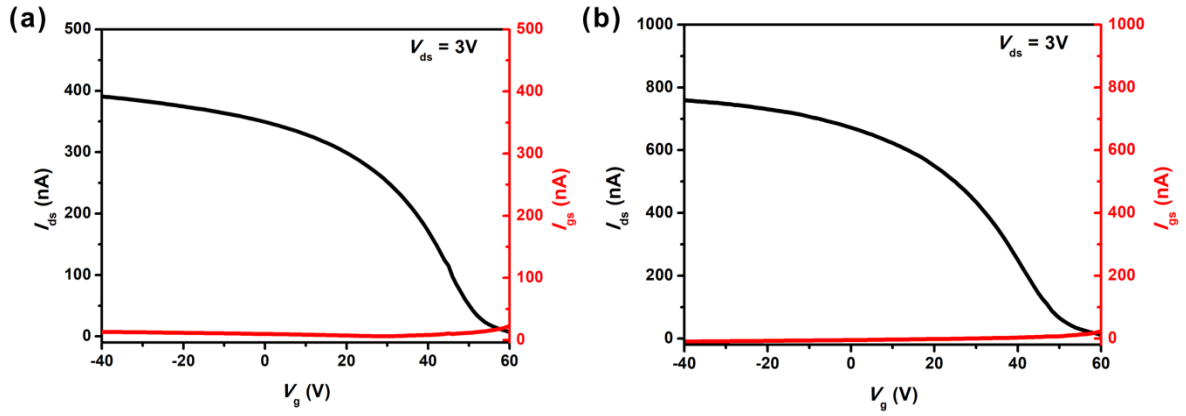

Figure S10. Comparison of the I_{ds} and gate leakage current (I_{gs}) for the devices fabricated with (a) 0.23% and (b) 0.48% Ag^{+} doped $CsPbBr_3$ NCs.

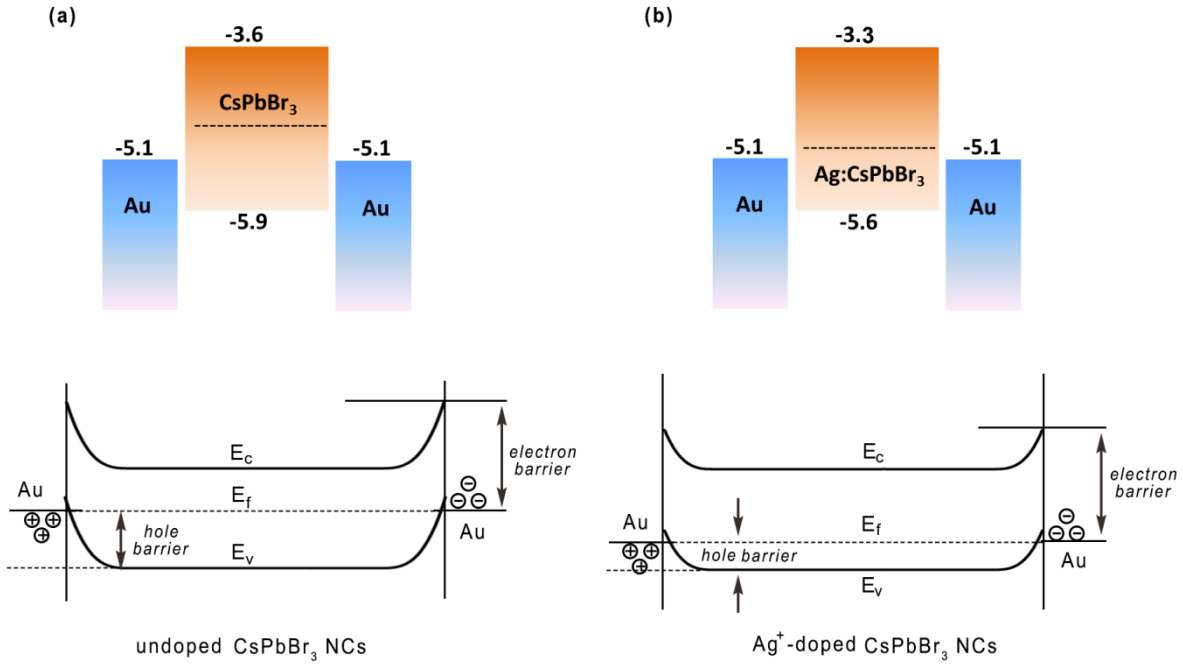

Figure S11. Band diagrams of the interface between the Au electrode and (a) undoped $CsPbBr_3$ NCs, and (b) Ag^+-doped $CsPbBr_3$ NCs. The electron barrier is correlated to the energy difference between the work function of the Au electrode and the affinition energy of $CsPbBr_3$ NCs. Whereas the hole barrier is correlated to the energy difference between the work function of the Au electrode and the ionization energy of $CsPbBr_3$ NCs.[6]

REFERENCES

(1) Liang, J.; Wang, C.; Wang, Y.; Xu, Z.; Lu, Z.; Ma, Y.; Zhu, H.; Hu, Y.; Xiao, C.; Yi, X.; *et al.* All-Inorganic Perovskite Solar Cells. *J. Am. Chem. Soc.* **2016**, *138*, 15829-15832.

(2) Begum, R.; Parida, M. R.; Abdelhady, A. L.; Murali, B.; Alyami, N. M.; Ahmed, G. H.; Hedhili, M. N.; Bakr, O. M.; Mohammed, O. F. Engineering Interfacial Charge Transfer in $CsPbBr_3$ Perovskite Nanocrystals by Heterovalent Doping. *J. Am. Chem. Soc.* **2017**, *139*, 731-737

(3) Diaconescu, B.; Padilha, L. A.; Nagpal, P.; Swartzentruber, B. S.; Klimov, V. I. Measurement of Electronic States of PbS Nanocrystal Quantum Dots Using Scanning Tunneling Spectroscopy: The Role of Parity Selection Rules in Optical Absorption. *Phys. Rev. Lett.* **2013**, *110*, 127406.

(4) Filip, M. R.; Hillman, S.; Haghighirad, A. A.; Snaith, H. J.; Giustino, F. Band Gaps of the Lead-Free Halide Double Perovskites $Cs_2BiAgCl_6$ and $Cs_2BiAgBr_6$ from Theory and Experiment. *J. Phys. Chem. Lett.* **2016**, *7*, 2579-2585.

(5) Liu, F.; Ding, C.; Zhang, Y.; Ripolles, T. S.; Kamisaka, T.; Toyoda, T.; Hayase, S.; Minemoto, T.; Yoshino, K.; Dai, S.; et al. Colloidal Synthesis of Air-Stable Alloyed $CsSn_{1-x}Pb_xI_3$ Perovskite Nanocrystals for Use in Solar Cells. *J. Am. Chem. Soc.* **2017**, *139*, 16708-16719.

(6) Tung, R. T. The Physics and Chemistry of The Schottky Barrier Height. *Appl. Phys. Rev.* **2014**, *1*, 011304.